Bioorganic & Medicinal Chemistry Letters 23 (2013) 1967–1973

Contents lists available at SciVerse ScienceDirect

Bioorganic & Medicinal Chemistry Letters

journal homepage: www.elsevier.com/locate/bmcl

# Triazolopyridazine LRRK2 kinase inhibitors

Maurizio Franzini [a,*], Xiaocong M. Ye [a], Marc Adler [b], Danielle L. Aubele [a], Albert W. Garofalo [a], Shawn Gauby [c], Erich Goldbach [c], Gary D. Probst [a], Kevin P. Quinn [c], Pam Santiago [c], Hing L. Sham [a], Danny Tam [d], Anh Truong [a], Zhao Ren [d]

[a] Department of Medicinal Chemistry, Elan Pharmaceuticals, 180 Oyster Point Blvd, South San Francisco, CA 94080, United States
[b] Department of Molecular Design, Elan Pharmaceuticals, 180 Oyster Point Blvd, South San Francisco, CA 94080, United States
[c] Department of Drug Metabolism and Pharmacokinetics, Elan Pharmaceuticals, 180 Oyster Point Blvd, South San Francisco, CA 94080, United States
[d] Department of Assay Development, Elan Pharmaceuticals, 180 Oyster Point Blvd, South San Francisco, CA 94080, United States

ARTICLE INFO

*Article history:*
Received 13 December 2012
Revised 1 February 2013
Accepted 7 February 2013
Available online 14 February 2013

*Keywords:*
LRRK2
Parkinson's
Inhibition
Kinase
Treatment
Discovery
Wild-type
G2019S mutant
Phosphorylation
SAR
Activity
Selectivity
Bioisostere
Hinge
HTS
Oxidative metabolism
Binding mode
Synthesis

ABSTRACT

Leucine-rich repeat kinase 2 (LRRK2) has been implicated in the pathogenesis of Parkinson's disease (PD). Inhibition of LRRK2 kinase activity is a therapeutic approach that may lead to new treatments for PD. Herein we report the discovery of a series of [1,2,4]triazolo[4,3-*b*]pyridazines that are potent against both wild-type and mutant LRRK2 kinase activity in biochemical assays and show an unprecedented selectivity towards the G2019S mutant. A structural rational for the observed selectivity is proposed.



Mutations in most genes associated with Parkinson's disease (PD) have been correlated with early onset or pathologically atypical forms of the disease. A recently identified PD-associated PARK gene that encodes for leucine-rich repeat kinase 2 (LRRK2) has been related to late onset PD[1] and has been indicated as the single most prevalent cause of monogenic PD.[2] Because the clinical phenotype deriving from *LRRK2* mutations is very similar to idiopathic PD, LRRK2 has emerged as one of the most relevant targets for pharmacological intervention in PD pathogenesis.[3] Mutations in LRRK2 are dominantly inherited and several have been shown to enhance kinase activity.[4] The most prevalent, causative LRRK2 mutation, G2019S, located in the kinase activation loop, leads to a two- to threefold in vitro increase in kinase activity.[5] Acute over-expression of G2019S LRRK2 can be toxic in SH-SY5Y neuroblastoma cells of primary cortical neurons.[6] Other experiments have shown that over-expression of mutant LRRK2 negatively impacts neurite outgrowth.[7] Although a few research groups have reported on new LRRK2 small molecule inhibitors,[8] to the best of our knowledge no prior work has been published on the selective inhibition of G2019S LRRK2. These observations have enticed us to pursue the development of novel mutant G2019S LRRK2 kinase inhibitors as potential new therapeutic agents for the treatment of PD.

At the onset of our efforts in this project, we screened an in-house kinase inhibitor focused library of compounds as an expedient way to find LRRK2 inhibitor classes. The screen used an

* Corresponding author.
*E-mail addresses:* mauriziof@alumni.stanford.edu, mfranzini@berkeley.edu (M. Franzini).

0960-894X/$ - see front matter © 2013 Elsevier Ltd. All rights reserved.
http://dx.doi.org/10.1016/j.bmcl.2013.02.043

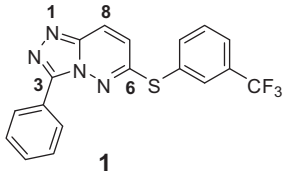

**1**

LRRK2$_{wt}$ $IC_{50}$= 0.242 μM
LRRK2$_{GS}$ $IC_{50}$= 0.050 μM
wt/G2019S = 4.8
Av. solubility 9 μM

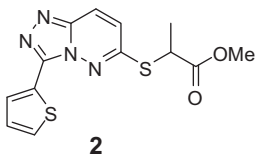

**2**

LRRK2$_{wt}$ $IC_{50}$= 0.535 μM
LRRK2$_{GS}$ $IC_{50}$= 0.200 μM
wt/G2019S = 2.7
Av. solubility 72 μM

**Figure 1.** Initial leads.

homogeneous time-resolved fluorescence (HTRF) assay measuring the inhibition of phosphorylation of LRRKtide.[9] A series of 3-aryl-6-arylthio-[1,2,4]triazolo[4,3-*b*]pyridazines emerged from the high throughput (HTS) screen as leads. Compound **1** was attractive due to its low molecular weight (<400) and encouraging in vitro potency with an interesting mutant (G2019S) versus wild type (wt) selectivity (Fig. 1). A test on a re-synthesized batch of **1** in a time-resolved fluorescence resonance energy transfer (TR-FRET) assay confirmed a biochemical potency of 0.242 μM in wt LRRK2 and 0.050 μM in G2019S LRRK2, with an inhibition ratio of 4.8 in favor of the mutant kinase. Most remarkably, compound **1** emerged as a selective kinase inhibitor for LRRK2. This compound was tested against a panel of 40 selected kinases in a single-point inhibition assay at 1 μM and found to cleanly inhibit LRRK2 with no other kinase in the test panel showing inhibition over 18%.[10] These preliminary promising results spurred our efforts into building an SAR with the goal of further optimizing the activity profile of this scaffold while improving the low solubility[11] and the poor permeability (21 nm/s) for **1**, which was on the same order of magnitude as poor permeability control atenolol (6 ± 3 nm/s).

HTS lead **2** showed comparable activity also in preference for G2019S LRRK2 along with higher solubility. A negligible P-gp liability (efflux ratio of 0.8) was observed for **2**, which was also very permeable (280 nm/s) and comparable to the high permeability control propranolol (170 ± 50 nm/s). These properties represented a significant improvement over **1**. The replacement of the phenyl ring at C-3 on compound **1** with a bioisosteric 2-thienyl group enhanced potency which is clearly seen when compound **3** is compared with **1** (Fig. 2). This was found to be a general trend in a

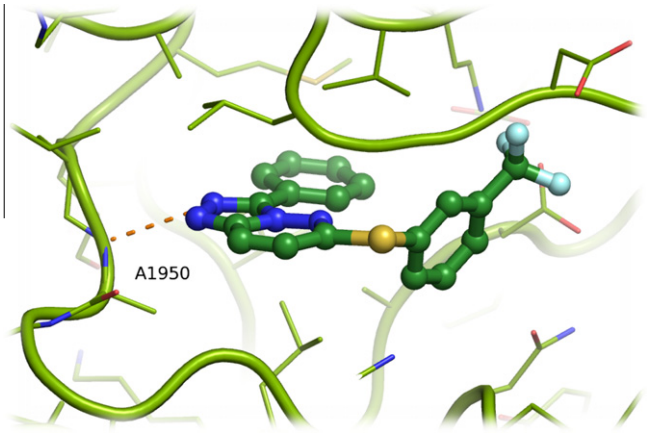


**Figure 3.** Homology model showing the proposed binding mode of **1** in the ATP pocket of the LRRK2 kinase domain.

series of 3-thienyl analogs (vide infra). We opted to maintain this moiety while investigating the effect of N-atom deletions in the fused heterocyclic core (Fig. 2). Of all variations tested, only imidazo[1,2-*b*] pyridazine **4** maintained comparable activity to the triazolo[4,3-*b*]pyridazine analog **3**. The most potent compound prepared during the early stages of HTS lead expansion was the corresponding 6-alkylthio derivative **8**, with a 7.6:1 G2019S/wt selectivity, a result that could be attributed to a potentially stronger interaction with the hinge binding region through the N-1 atom within the imidazole moiety. However, compound **8** suffered from a surprising loss of selectivity as measured in a representative kinase panel; therefore this core modification was not pursued any further.

Our homology model of LRRK2 binding was developed on the basis of MLK1 (pdb ID: 3DTC).[12] At the time, the 3DTC structure had the closest homology to LRRK2 as judged by the BLAST score (1e-25, with 31% identities). However, the 3DTC contained several ligand induced conformational changes that were undesirable. These included a collapsed P-loop and a partially disordered DFG sequence. The P-loop was remodeled using homologous structures of kinases with ATP analogues. The DYG sequence was built to resemble PKC-ι (pdb ID: 3A8X), one of the few pdb kinase structures that contain a DYG sequence.[13] We propose that compound

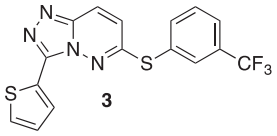

**3**

LRRK2$_{wt}$ $IC_{50}$ = 0.075 μM
LRRK2$_{GS}$ $IC_{50}$ = 0.023 μM
wt/G2019S = 3.3
Av. solubility = 8 μM

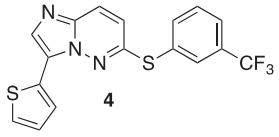

**4**

LRRK2$_{wt}$ $IC_{50}$ = 0.101 μM
LRRK2$_{GS}$ $IC_{50}$ = 0.047 μM
wt/G2019S = 2.1
Av. solubility = 14 μM

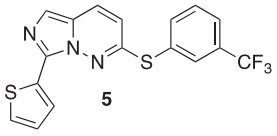

**5**

LRRK2$_{wt}$ $IC_{50}$ = 10.66 μM
LRRK2$_{GS}$ $IC_{50}$ = 7.27 μM
wt/G2019S = 1.5
Av. solubility = 10 μM

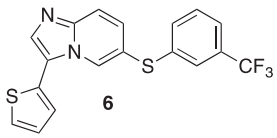

**6**

LRRK2$_{wt}$ $IC_{50}$ = 4.215 μM
LRRK2$_{GS}$ $IC_{50}$ =1.313 μM
wt/G2019S = 3.2
Av. solubility = 11 μM

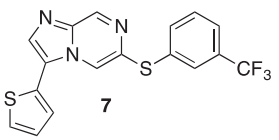

**7**

LRRK2$_{wt}$ $IC_{50}$ = 3.400 μM
LRRK2$_{GS}$ $IC_{50}$ = 2.168 μM
wt/G2019S = 1.6
Av. solubility = 18 μM

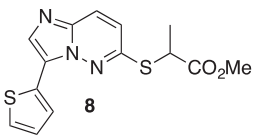

**8**

LRRK2$_{wt}$ $IC_{50}$ = 0.076 μM
LRRK2$_{GS}$ $IC_{50}$ = 0.010 μM
wt/G2019S = 7.6
Av. solubility = 35 μM

**Figure 2.** Variations on the scaffold core.

**Table 1**
Variations on the C-3 heterocyclic substituent

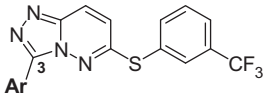

| Compd | Ar | LRRK2 wt $IC_{50}$ (μM) | LRRK2 G2019S $IC_{50}$ (μM) | wt/G2019S |
|---|---|---|---|---|
| **9** | 1*H*-Pyrazol-5-yl | 0.053 | 0.013 | 4.1 |
| **10** | Thiazol-5-yl | 0.074 | 0.018 | 4.1 |
| **11** | Thiazol-2-yl | 0.088 | 0.025 | 3.5 |
| **12** | Thiazol-4-yl | 0.140 | 0.035 | 4.0 |
| **13** | 3-Bromothiophen-2-yl | 0.613 | 0.134 | 4.6 |
| **14** | Pyridin-2-yl | 0.164 | 0.045 | 3.6 |
| **15** | Pyridin-3-yl | 0.211 | 0.064 | 3.3 |
| **16** | Pyridin-4-yl | 0.859 | 0.253 | 3.4 |
| **17** | 2-Chlorophenyl | 3.305 | 1.023 | 3.2 |
| **18** | 3-Chlorophenyl | 0.265 | 0.051 | 5.2 |
| **19** | 3-(Piperazin-1-yl)phenyl | 0.314 | 0.055 | 5.7 |
| **20** | 4-Fluorophenyl | 0.674 | 0.179 | 3.8 |

**Table 2**
Aliphatic variations on C-3

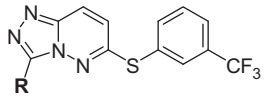

| Compd | R | LRRK2 wt $IC_{50}$ (μM) | LRRK2 G2019S $IC_{50}$ (μM) | wt/G2019S |
|---|---|---|---|---|
| **21** | Cyclopropyl | 0.994 | 0.309 | 3.2 |
| **22** | Cyclopentyl | 1.549 | 0.511 | 3.0 |
| **23** | Tetrahydro-2*H*-pyran-4-yl | 5.329 | 2.020 | 2.6 |
| **24** | Piperidin-4-yl | >20 | 22.128 | – |
| **25** | Thiophen-2-ylmethyl | >20 | 19.542 | – |

**Table 3**
Variations on the C-6 arylthio substituent

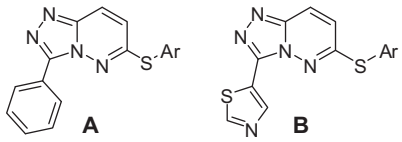

| Compd | Series | Ar | LRRK2 wt $IC_{50}$ (μM) | LRRK2 G2019S $IC_{50}$ (μM) | wt/G2019S |
|---|---|---|---|---|---|
| **26** | A | 4-(Trifluoromethyl)phenyl | 5.897 | 2.026 | 3.0 |
| **27** | A | 2-(Trifluoromethyl)phenyl | 3.168 | 2.470 | 1.3 |
| **28** | B | 3-Bromophenyl | 0.032 | 0.006 | 5.3 |
| **29** | B | 3-Chlorophenyl | 0.031 | 0.008 | 3.9 |
| **30** | B | 3-Fluorophenyl | 0.169 | 0.077 | 2.2 |
| **31** | B | 3-Methoxyphenyl | 0.138 | 0.026 | 5.3 |
| **32** | B | 3-*tert*-Butylphenyl | 0.075 | 0.030 | 2.5 |
| **33** | B | 3-(Trifluoromethoxy)phenyl | 0.281 | 0.067 | 4.2 |
| **34** | B | pyrimidin-2-yl | 0.117 | 0.101 | 1.2 |
| **35** | B | 4-(Trifluoromethyl)pyrimidin-2-yl | 0.183 | 0.033 | 5.5 |
| **36** | B | Phenyl | 0.159 | 0.141 | 1.1 |

**1** binds to the kinase domain of LRRK2 as shown in Figure 3, where the most relevant interaction is a H-bond in which the triazolo ring accepts a H-bond from hinge residue A1950.

A variety of compounds with different aryl, heteroaryl, and alkyl groups on C-3 were prepared and tested, while maintaining the 3-(trifluoromethyl)phenylthio substituent on C-6, as shown in Tables 1 and 2.[14] We observed that five-membered heterocycles with a variety of substitution patterns (e.g., **9** through **12**) were generally more potent than six-membered rings (e.g., **14** through **20**). In all cases selectivity in favor of the inhibition of mutant LRRK2 is preserved. Of comparable potency to this subclass of compounds, the 2-pyridyl derivative **14** suggests a potential role played by the dihedral

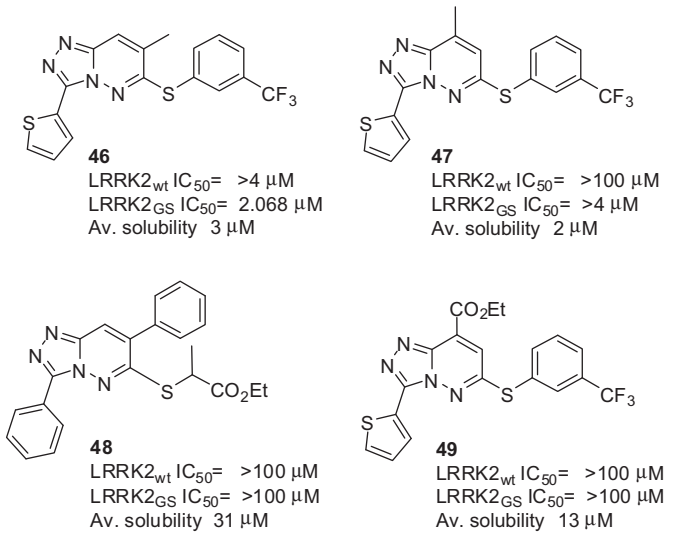


**Figure 4.** C-7 and C-8 substituted analogs.

angle between the C-3 heteroaryl group and the [1,2,4]triazolo[4,3-*b*]pyridazine core. Indeed, although G2019S $IC_{50}$ values for parent compound **1** and *meta*-substituted derivatives **18** and **19** are very close to the corresponding values for **14** (within standard deviation), *ortho*-substitution on the phenyl ring, such as that seen in **17**, induced a 10- to 20-fold decrease in potency. Similarly, 3-bromo-2-thienyl derivative **13** showed a six- to eightfold decrease in potency as compared to **3**. Conversely, minor substitutions at the *para* position on the phenyl ring, such as the fluorine in **20**, come with a threefold decrease in potency, suggesting a tight space within the enzyme pocket surrounding the phenyl ring on C-3. The presence of a hydrogen bond acceptor at the *para* position was not favorable either, as shown by a further decrease in potency with compound **16** (to be compared with **14** and **15**).

Small cycloalkyl groups at C3, such as the cyclopropane ring in **21** or the cyclopentane in **22**, are detrimental to potency (Table 2). Modest expansion to a THP ring, as in **23**, further reduces potency by a factor of 3 to 4. The presence of a H-bond donor, as in piperidine analog **24**, completely erased kinase inhibition; the same effect was observed upon introduction of a one-carbon linker between the core and the thienyl ring (**25**).

Concerning the substitution pattern on the thioaryl group linked to C-6, the *meta* position of the trifluoromethyl substituent seemed highly preferred (compare **26** and **27** with **1**, Table 3). Most rewardingly, the combination of a C-3 thiazole and a C-2 3-halophenylthioether afforded compounds in this series (**28, 29**) with single digit nanomolar potency against mutant LRRK2 while maintaining selectivity vs. wild type LRRK2. This gain in potency was not preserved in the *meta*-fluoro analog **30**, an indication that steric bulk and polarizability of the substituent in this position might be relevant factors to maintaining potency. Electron-donating and withdrawing groups, as in **31** and **33**, respectively, or bulkier groups, as in **32**, seemed well tolerated. Introduction of heteroatoms in the arylthio ring, to give for instance pyrimidine derivative **35**, only marginally affected potency. Exclusion of ring substituents, as in **34** or **36**, reduced potency especially against the mutant, thus erasing the selectivity gained in most other cases, an intriguing finding in our SAR.

As with HTS hit **2**, and in contrast to the observed trend with substitution on the left-hand side of the molecule, the aryl group linked to C-6 via the sulfide can be replaced by a polar aliphatic chain, featuring an ester or a primary amide (Table 4). In this series, primary amide **37** was of comparable potency to aryl analog **3** although the mutant vs. wild type $IC_{50}$ ratio suffered significant erosion. This observation supported the assumption that hydrophobic, aromatic functionality in a specific orientation was necessary for optimal inhibition of the G2019S mutant kinase. When tested in a 40-kinase panel at 1 μM, **37** (solubility = 12 μM) showed the same excellent selectivity for LRRK2 as seen for **1**. Methyl ester **38** was found to be about fivefold less potent than the corresponding amide, **37**. The configuration of the stereocenter in **38** does not seem to be relevant, in that enantiomers **39** and **40** were virtually equipotent. Simple homologation of the alkyl substituent, as in **41**, also did not change the $IC_{50}$ significantly. However, further branching into an isopropyl group (as in **42**) depressed potency. Incorporation of a quaternary α-carbon (**43**) strongly reduced activity, and virtually erased any wt vs. mutant selectivity. Isosteres of the carboxylate functionality, such as oxadiazole **44** and pyrazole **45**, proved only marginally beneficial. The average kinetic solubility of C-6 alkylthio analogs was significantly improved for some ester derivatives (99 μM for **39**, as a representative example) and for heterocyclic isosteres (88 μM for **44**), but remained low for primary amides (12 μM for **37**).

With the intent to probe the available space surrounding C-7 and C-8, 7- and 8- methyl substituted derivatives of **3** (**46** and **47**, respectively) were prepared and found to be virtually inactive, so were analogs **48** and **49** (Fig. 4), an indication of the possible tight packing in the binding pocket around this region. Further evidence for a constrained binding pocket came from the observed inactivity of a series of analogs in which the thioether was replaced. Modeling suggests that the dihedral angle around the thioether should be close to 90°. Analogs incorporating O, as in **50**, N, as in **51**, or C, as in **52** and **53**, should have a wider dihedral angle and all were substantially less active (Table 5).

Oxidative metabolism soon emerged as a major liability with the large majority of all the compounds in the sulfide series. Incubation of **1** in NADPH-supplemented rat liver microsomes at 37 °C for 30 min completely consumed the parent molecule resulting in the putative sulfoxide **54** and sulfone **55** metabolites. However, this oxidation pathway was less extensive in human liver microsomes. The latter compounds were independently synthesized, tested, and found to be very weak inhibitors (Fig. 5). They were also significantly more resistant to degradation in the microsomal stability assays. The replacement of the arylthio moiety with carbon-based and small heterocyclic bioisosteric groups is the focus of current synthetic efforts.

In regard to a cellular assay, inhibition of LRRK2 kinase is known to decrease autophosphorylation at S935. This measurement can be utilized to assess LRRK2 kinase activity in cells.[15] Our cellular assay employed HEK293 cells stably transfected with LRRK2 (G2019S). Several compounds exhibited better than 1 μM potency and we observed some correlation with in vitro biochemical results, although with a 100-fold discrepancy possibly due to poor permeability (Table 6).

## Synthesis

Based on several experimental findings that emerged during our synthetic efforts, intermediate **59** behaves more like an acyl chloride than as an aryl halide due to the high electron deficiency of the fused heterocycle. Displacement by good nucleophiles, such thiophenates and thiolates, typically occur under mild conditions in the presence of inorganic weak bases (rt–80 °C) to give the target sulfides in generally good yield.

As a representative example, synthesis of compound **21** from pyridazine **56** is shown in Scheme 1. The preparation of C-3 (hetero)aryl derivatives (such as **3**) can take advantage of an expeditious one-pot cyclocondensation of 3,6-dichloropyridazine **61**

**Table 4**
Variations on the C-6 alkylthio substituent

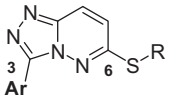


| Compd | Ar | R | LRRK2 wt $IC_{50}$ (μM) | LRRK2 G2019S $IC_{50}$ (μM) | wt/G2019S |
|---|---|---|---|---|---|
| **37** | 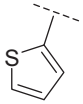 | 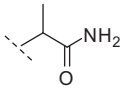 | 0.098 | 0.048 | 2.0 |
| **38** |  | 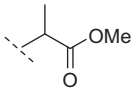 | 0.535 | 0.200 | 2.7 |
| **39** |  | 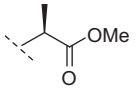 | 0.458 | 0.215 | 2.1 |
| **40** |  | 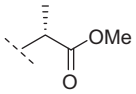 | 0.463 | 0.187 | 2.5 |
| **41** |  | 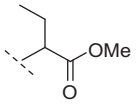 | 0.338 | 0.167 | 2.0 |
| **42** |  | 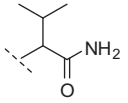 | 1.294 | 0.581 | 2.2 |
| **43** | 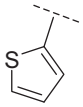 | 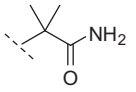 | 2.420 | 3.117 | 0.8 |
| **44** |  | 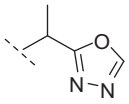 | 0.384 | 0.162 | 2.4 |
| **45** | 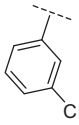 | 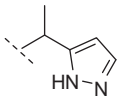 | 1.662 | 0.798 | 2.1 |

**Table 6**
Selected cell activity values

| Compd | LRRK2 G2019S $IC_{50}$ (μM) | G2019S S935 cell $IC_{50}$ (μM) |
|---|---|---|
| **3** | 0.023 | 1.656 |
| **9** | 0.013 | 1.016 |
| **10** | 0.018 | 0.780 |
| **11** | 0.025 | 1.727 |
| **12** | 0.035 | 2.112 |
| **28** | 0.006 | 0.683 |
| **29** | 0.008 | 1.397 |
| **32** | 0.030 | 1.393 |
| **37** | 0.048 | 3.032 |

with a hydrazide (**62**), to give the corresponding C-6 chloride (**63**) in good yield. Disappointingly, transition-metal catalyzed cross coupling of chlorides such as **63** with boronic acids and their derivatives (Suzuki conditions) generally proved challenging and low-yielding at best, mostly due to competitive hydrolysis of the C-6 chloride.

Installment of substituents at C-7 (as in **48**) required the regioselective functionalization of a 3-phenyl-6-chloro-[1,2,4]triazolo[4,3-*b*]pyridazine **61** via Knochel's zincation with TMPZnCl·LiCl, Scheme 2.[16] Substituents at C-8 (as in **47** and **49**) had to be introduced at the onset of the synthetic route, on the 3,6-dichloropyridazine starting material.

On a number of cases, significant amounts of bis-thiolated side-products were isolated whereby position C-8 was found decorated with the thiol utilized for the substitution on the C-6 position. Such unusual reactivity on C-8 can be rationalized by partial charges computation on the [1,2,4]triazolo[4,3-*b*]pyridazine core, and is described in the literature to occur via a vicarious nucleophilic substitution.[17]

In summary, we have designed and synthesized a series of [1,2,4]triazolo[4,3-*b*]pyridazines that are potent and selective LRRK2 inhibitors. A homology model of LRRK2 binding was proposed and an inhibitor binding mode postulated based on this model. An SAR campaign was developed giving rise to a series of compounds with unprecedented selectivity for the inhibition of LRRK2 (G2019S) over wild type LRRK2. In particular, analogs **28** and **29** gave single digit nM inhibition in the biochemical assay,

**Table 5**
Variations on the C-6 linker

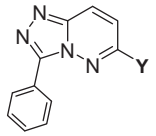

| Compd | Y | LRRK2 wt $IC_{50}$ (μM) | LRRK2 G2019S $IC_{50}$ (μM) |
|---|---|---|---|
| **50** | 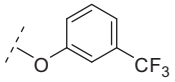 | >4 | 1.555 |
| **51** | 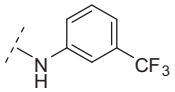 | >100 | >100 |
| **52** | 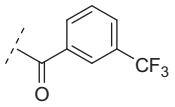 | 25 | 4.57 |
| **53** | 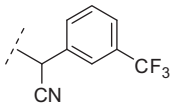 | 26 | 18 |

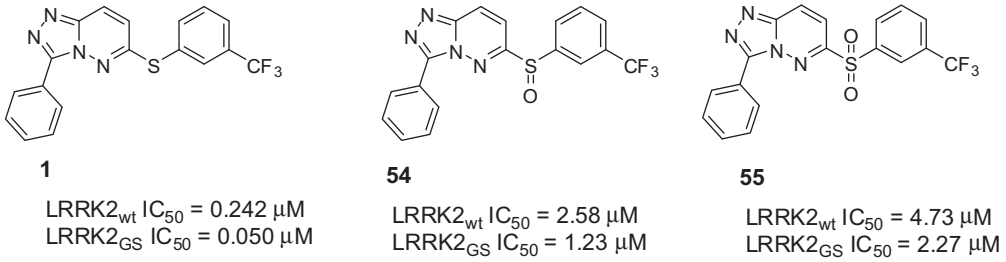


**Figure 5.** Metabolic oxidation of **1** to sulfoxide (**54**) and sulfone (**55**).

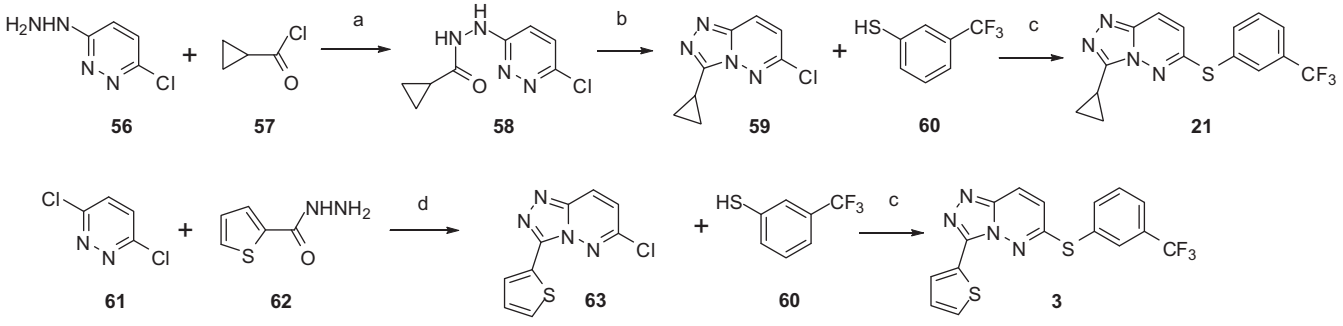


**Scheme 1.** Reagents and conditions: (a) $Et_3N$, $CH_2Cl_2$, rt, 85%; (b) HOAc, 100 °C, 68%; (c) $K_2CO_3$, DMF, 80 °C, 87%; (d) $Et_3NHCl$, $C_6H_5CF_3$, 140 °C, 65%.

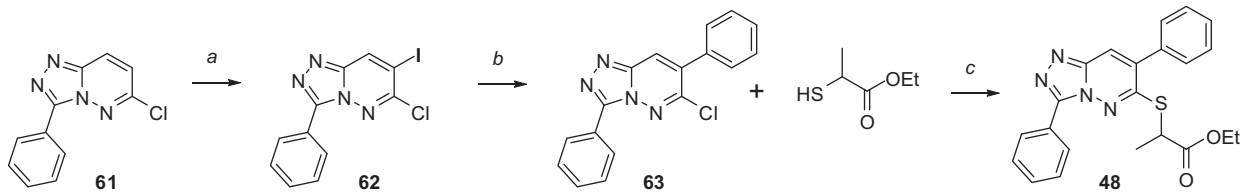


**Scheme 2.** Reagents and conditions: (a) TMPZnCl·LiCl, THF, rt; then $I_2$, rt, 57%; (b) $PhB(OH)_2$, cat $[Pd(dppf)Cl_2]$, 2 M $Na_2CO_3$, DME, 90 °C, 35%; (c) $K_2CO_3$, rt, 77%.

and showed interesting potency in the cell-based assay. However, the poor oxidative metabolic stability of this series could not be overcome despite our efforts, thus preventing the in vivo testing of the compounds. As a result of these limitations, further medicinal chemistry efforts on this series have been suspended.

## Acknowledgments

The authors thank Wayman Chan for performing difficult purifications. We also want to acknowledge the work of Pui Seto, Monica You, Jeanne Baker, and Kevin Tanaka for the production and purification of antibodies used in our assays.

## References and notes

1. Paisan-Ruiz, C. et al *Neuron* **2004**, *44*, 595; Zimprich, A. et al *Neuron* **2004**, *44*, 601.
2. Paisan-Ruiz, C.; Nath, P.; Washecka, N.; Gibbs, J. R.; Singleton, A. B. *Hum. Mutat.* **2008**, *29*, 485.
3. Wang, G.; Pan, J.; Chen, S.-D. *Prog. Neurobiol.* **2012**, *98*, 207.
4. Vancraenenbroeck, R.; Lobbestael, E.; De Mayer, M.; Baekelandt, V.; Taymans, J.-M. *CNS Neurol. Disord. Drug Targets* **2011**, *10*, 724.
5. Greggio, E.; Cookson, M. R. *ASN Neuro.* **2009**, *1*; West, A. B.; Moore, D. J.; Choi, C.; Andarbi, S. A.; Li, X.; Dikeman, D.; Biskup, S.; Zhang, Z.; Lim, K. L.; Dawson, V. L.; Dawson, T. M. *Hum. Mol. Genet.* **2007**, *16*, 223.
6. Smith, W. W.; Pei, Z.; Jiang, H.; Moore, D. J.; Liang, Y.; West, A. B.; Dawson, V. L.; Dawson, T. M.; Ross, C. A. *Proc. Natl. Acad. Sci. U.S.A.* **2005**, *105*, 18676.
7. Wang, L.; Xie, C.; Greggio, E.; Parasiadou, L.; Shim, H.; Sun, L.; Chandran, J.; Lin, X.; Lai, C.; Yang, W. J.; Moore, D. J.; Dawson, T. M.; Dawson, V. L.; Chiosis, G.; Cookson, M. R.; Cai, H. *J. Neurosci.* **2008**, *28*, 3384.
8. See, for instance. Chen, H.; Chan, B.; Drummond, J.; Estrada, A. A.; Gunzner-Toste, J.; Liu, X.; Liu, Y.; Moffat, J.; Shore, D.; Sweeney, Z.; Tran, T.; Wang, S.; Zhao, G.; Zhu, H.; Burdick, D. *J. Med. Chem.* **2012**, *55*, 5536; Also: Reith, A. D.; Bamborough, P.; Jandu, K.; Andreotti, D.; Mensah, L.; Dossang, P.; Choi, H. G.; Deng, X.; Zhang, J.; Alessi, D. R.; Gray, N. S. *Bioorg. Med. Chem. Lett.* **2012**, *22*, 5625.
9. Homogeneous time-resolved fluorescence (HTRF) assay using GST-LRRK2. Detection was done using biotinylated LRRKtide, Eu(K)-Ab (p-Moesin)/SA-XL665 measured at 620 and 665 nm.
10. Compounds were tested at Invitrogen in a single-point assay. Selected tested kinases included Abl1, Akt1, Aurora A, CDK1/cyclin B, CDK5/p25, Chek 1, CSF1R (Fms), ErbB4 (Her4), Flt3, GSK3β, Jak1, various MAPKs, PDGFRα, PIK3CA (p110α), PLK1 through 3, Raf1 (cRAF), Ret, Syk, Ttk.
11. Kinetic solubility, measured in isotonic buffer at pH 7.4, average of two determinations.
12. Hudkins, R. L.; Diebold, J. L.; Tao, M., et al *J. Med. Chem.* **2008**, *51*(18), 5680.
13. Takimura, T.; Kamata, K.; Fukasawa, K., et al *Acta Crystallogr., Sect. D* **2010**, *D66*, 577.
14. Enzyme activity was determined using GST-LRRK2(970-2527), GST-(G2019S)LRRK2(970-2527), and LRRKtide in the presence of 100 μM ATP.
15. Dzamko, N.; Deak, M.; Hentati, F., et al *Biochem. J.* **2010**, *430*, 405.
16. Mosrin, M.; Knochel, P. *Org. Lett.* **2009**, *11*, 1837; Bresser, T.; Mosrin, M.; Monzon, G.; Knochel, P. *J. Org. Chem.* **2010**, *75*, 4686.
17. Katriusiak, A. A. et al *Pol. J. Chem.* **1996**, *70*, 1279. *Tetrahedron Lett.* **2006**, *47*, 4259.